Ann. Geophys. Discuss.,
https://doi.org/10.5194/angeo-2020-47-AC2, 2020

Annales Geophysicae Discussions
Open Access

Interactive comment on "Migrating tide climatologies measured by a high-latitude array of SuperDARN HF-radars" *by* Willem E. van Caspel et al.

Willem E. van Caspel et al.

willem.e.v.caspel@ntnu.no

Received and published: 29 September 2020

The authors would like to thank the reviewer for their comments on our work. We address each comment individually by stating the original Referee Comment (RC) followed by the Author's Response (AR).

RC1: Page 1, line 14: Perhaps replace the term "Hough" (which will be unfamiliar to most readers) with "spherical harmonic"?

AR1: The authors agree with RC1 in that latitudinal spherical harmonic structures (associated Legendre polynomials) will be more familiar to most readers. However,

Printer-friendly version

Discussion paper

since Hough modes form such an integral part of tidal theory (as described in detail in the work of Chapman and Lindzen (2012) cited on line 13), and because Hough modes are also referred to in the discussion, we would still like to make reference to Hough modes in our introduction of the tides. Since both spherical harmonics and Hough modes can be expressed as a combination of either one, as both form a complete set of basis functions, we think the following change to line 14 in the revised manuscript may offer more clarity:

“The tides have a latitudinal spherical harmonic structure (termed Hough modes) and longitudinal zonal wavenumber (S) structure,...”

RC2: Page 1, line 23: “yaw cycle intermittency” sounds wordy and opaque. Replace with “slow local time precession”.

AR2: Line 23 has been rewritten to include slow local time precession as a drawback of satellite measurements, while still including yaw cycle maneuvers (e.g., the changing latitudinal coverage of SABER/TIMED every 60 days, and every 36 days for MLS/UARS) as a separate drawback. Line 23 now reads:

“Typical drawbacks associated with satellite measurements arise due to constraints imposed by asynoptic sampling (Salby, 1982), including slow local time precession and yaw cycle maneuvers.”

RC3: Page 4, lines 76-77: This sentence is incomprehensible. Are you trying to say that “If measurements are not available for both stations at any given time, measurements are excluded in a manner so as to optimize the equidistant longitudinal spread of measurements?”

AR3: It was our intention to say that, if measurements are available for two closely-spaced (in longitude) stations at any given time, we leave out one of the station’s measurements in the fit to Eq. 1, such that the longitudinal spread of measurements becomes more equally spaced over the fitting domain.

For example, if at a certain time there are measurements available from Han, Pyk, Sto, Gbr, Sas and Kod (as shown in Fig. 1), the measurement of Pyk is excluded in the fit to Eq. 1. If we didn't exclude Pyk, the winds measured at the longitude corresponding to the (Sto, Pyk) 'longitude pair' would effectively have a double weight in the least-squares fitting routine, which is undesirable. The measurement of Pyk is therefore excluded in the fit, since the fit is then applied only to measurements that are spaced roughly 50 degrees longitude apart. In the revised manuscript, lines 76-77 have been rewritten to,

"To that end, for the radar pairs closely spaced in longitude, (Ksr, Kod), (Rnk, Kap), and (Sto,Pyk), only one of each of the pairs measurements is used in the fit to Eq. 1, even if data are available for both.".

RC4: Figures 2-5 need to be enlarged.

AR4: Figures 2-5 have been enlarged as well as modified in accordance with the comments of Reviewer 1.

RC5: I suggest showing the climatology first, then the year to year variability.

AR5: We followed the plan of similar climatological papers, where the raw data, with its variability, is presented first. The climatology is then shown to emphasize that only the seasonal variations present in the data have been isolated in the climatology. We then go on to discuss only those features observed in the climatology and draw conclusions from them. If we reverse the order, the flow jumps from climatology, to raw data, to discussing the climatology. While we could reverse the order without prejudicing the results, we would prefer to keep the present order to reflect other climatology papers and to provide a better "readability" factor.

RC6: Page 7, line 151: replace "tidal modes" with "tides".

AR6: "tidal modes" has been replaced with "tides" throughout the text in accordance with RC11.

RC7: Page 8, lines 155-156: Simplify to: "...not lead to significant cross-contamination errors between the migrating tides."

AR7: Lines 155-156 have been simplified in accordance with RC7.

RC8: Figure 6: Any idea why the RMS difference for SW2 is so much higher than the others?

AR8: We are unable to identify any particular reason why SW2 has a RMSE roughly 50% greater than that of DW1 and TW3. For example, no one-to-one relation exists between the yearly mean tidal amplitudes in NAVGEM-360 (9.8, 10.1, and 2.74 ms-1 for DW1, SW2, and TW3, respectively) and the yearly mean RMSE values shown in Figure 6.

RC9: Page 10, line 187: "Should read "Whether conditions are favourable..."

AR9: Line 187 has been updated in accordance with RC9.

RC10: Page 10. The nomenclature is confusing. (1,1) is the first symmetric propagating Hough mode. (1,2) is the first antisymmetric propagating mode.

AR10: For consistency, we now refer to the diurnal (1,1) mode in the same manner as Dhadly et al. 2018, which is the work cited in our discussion on the DW1 tide. The mode is now simply referred to as the Diurnal (1,1) Hough-mode.

RC11: The term "mode" refers to the latitudinal structures, or Hough modes. It should not be used to describe the longitudinal wavenumber or frequency. Thus, DW1, SW2, etc. are tides. (1,1) is a mode.

AR11: "tidal modes" has been replaced with "tides" throughout the text to correctly reflect the distinction between the latitudinal Hough mode structure and longitudinal wavenumber structure of atmospheric tides.

RC12: Page 10, lines 195- 208. Lots of speculation here about the diurnal winds and how they may be distorted by the SuperDARN "observational filter". Is it feasible to quantify these effects by forward modeling DW1 winds into meteor echoes?

AR12: The various factors that might impact the representation of DW1 in the SuperDARN meteor winds have been further examined in the interim, and the vertical wavelength of DW1 being near to the vertical average represented by SuperDARN winds is likely to be the most impactful. Hence, to avoid unnecessary speculation, the following lines have been removed from the text:

“In addition, DW1 is the tide most susceptible to contamination by non-migrating tides, given that the 180 degrees of longitude aliases DW1 and the diurnal oscillation in the mean wind (D0). Although no evidence of such cross-contamination is found in the NAVGEM-HA sampling experiments, with D0 amplitudes in NAVGEM-360 never reaching above 4.0 ms-1. Lastly, DW1 is likely to be the tide that is most strongly affected by the diurnal cycle of meteor echoes (Hussey et al., 2000;Tsutsumi et al., 2009).“

The quantify the effect of the vertical average “observational filter” of SuperDARN would require the model top of the NAVGEM-HA meteorological analysis system to be extended at least up to ∼125 km altitude. But as discussed in AR1 to the comments of reviewer 1, this is beyond the scope of the current work.

Interactive comment on Ann. Geophys. Discuss., https://doi.org/10.5194/angeo-2020-47, 2020.

Ann. Geophys. Discuss.,
https://doi.org/10.5194/angeo-2020-47-AC1, 2020

Annales Geophysicae Discussions
Open Access
EGU

Interactive comment on “Migrating tide climatologies measured by a high-latitude array of SuperDARN HF-radars” *by* Willem E. van Caspel et al.

Willem E. van Caspel et al.

willem.e.v.caspel@ntnu.no

Received and published: 3 September 2020

The authors would like to thank the reviewer for their comments on our work. We address each comment individually by stating the original Refereee Comment (RC) followed by the Author's Response (AR).

RC1: This is my main comment for this work. Do SuperDARN radar tides com- pare well with your model (NAVGWM-SD)? I saw NAVGEM-SD and NAVGEM -360 com- parison, and results look great. Authors mentioned in the section 2.3, NAVGEM – HA show good agreement with tides and winds from previous radars and satellite ob- ser- vations. I am wondering if your tides show good agreement with NAVGEM. Can you

Printer-friendly version

Discussion paper

add SuperDARN radar tidal results in Figure 5 along with NAVGEM-SD and NAVGEM-360? Or can you show us comparisons between modeling work and SuperDARN radar observed tides?

AR1: The purpose of including the NAVGEM-HA analysis was to validate the SuperDARN tidal analysis method. That is, that the combination of radars, each measuring the tidal oscillations at different locations, can be used to extract the unambiguous migrating components without bias due to the discrete spatial sampling of SuperDARN. We did not include a direct comparison between SuperDARN and NAVGEM-HA on the basis that the SuperDARN tides represent a broad vertical average (calculated from a Gaussian meteor echo distribution centered on ∼100 km altitude with a FWHM of 25-35 km), whereas NAVGEM-HA can be used up to an altitude of ∼90 km for tidal analysis. The SuperDARN meteor winds therefore represent tidal measurements of a region that is largely outside of the NAVGEM-HA model domain. A detailed comparison between the modeled and observed tides would require the model domain to be extended up to ∼ 125 km altitude below the sponge layer, such that vertically averaged model winds can be compared to those measured by SuperDARN. Nonetheless, we think the inclusion of the SuperDARN tidal modes in Figure 5, as suggested by the reviewer, is a worthwhile addition, not in the least because it demonstrates more clearly that the modeled and measured tidal modes share similar seasonal characteristics, further justifying the use of NAVGEM-HA to validate the SuperDARN tidal analysis method. The SuperDARN measurements have therefore been included in Figure 5 of the revised manuscript, and a brief description of the above reasoning has been included as a third paragraph in section 4.1.

RC2: It is hard to see where are DOY 250, 260, 365 etc mentioned in the page 4-5 for Figures 2-3. Also it is hard to see where is “late summer” and “mid-winter” from Figure 2 and 3. Would you add vertical lines for every year (currently every two years)? Can you also specify “late summer’ and “mid-winter”(which months are you talking about?).

AR2: Throughout the manuscript, text referring to certain time periods has been changed so as to be more clear about what time period is being referred to in Figures 2-4 (e.g., ‘mid-winter’ (December - January)). Vertical lines have been added for each year in Figures 2-3, and Figure 4 now shows DOY on its x-axis (see AR3).

RC3: Authors discussed a lot about DOY 260. Would you indicate DOY 260 in some of your figures? X-axis is years and it is hard to see from Figures 2-3.

AR3: The labeling on the x-axis of Figure 4 has been changed to Day Of Year (DOY), and a vertical line at DOY 265 is included in the bottom left panel showing the climatology of the amplitude of the migrating terdiurnal tide (TW3, bottom left panel). What was referred to as the DOY 260 amplitude peak is now referred to as the DOY 265 amplitude peak, to more precisely reflect its exact timing.

RC4: Figure 5: What are you plotting? Zonal wind? Or meridional wind? (I think it is zonal wind, but it is not clear).

AR4: Figure 5 plots the migrating tidal modes in the meridional wind, which is now clarified in the figure caption.

RC5: Authors discussed that radars can see high-temporal reso- lutions, resulting in the peak around DOY 260. Would you discuss more about this? What are temporal resolution of previous terdiurnal tide work?

AR5: To the best of the author’s knowledge, previous observational studies capable of unambiguously isolating the migrating component of the terdiurnal tide in the northern hemisphere mid- to high-latitude MLT region have exclusively relied on satellite observations. Such observations are limited to temporal resolutions of monthly timescales. For example, Smith (2000) combines UARS data over two yaw cycles (70 day average) to retrieve TW3 tidal amplitudes at 60N. As a result, features such as the DOY 265 maximum observed by SuperDARN are not distinguishable in their figure 2. Other studies capable of isolating the mid- to high-latitude migrating terdiurnal tide have used SABER/TIMED satellite data (e.g., Moudden et al., 2013; Pancheva et al., 2013), but in addition to being limited to 20- to 60-day means, they only report temperature tides, which further complicates the comparison with SuperDARN.

Model studies seem to show mixed results in terms of the temporal resolution of their tidal analysis and the effective temporal resolution of their results. The cited works by Akmaev (2001) and Smith et al. (2001) describe model results showing a qualitatively similar seasonal cycle as the observed SuperDARN TW3 (i.e., a broad amplitude maximum in the zonal and meridional winds during winter). These studies have used monthly mean specifications of the background atmosphere. For example, in Figure 2 of Smith et al. (2001), no DOY 265 peak is distinguishable at 97 km altitude. The study by Yue et al. (2013) employs a model that is configured using a mixture of daily mean and monthly mean atmospheric background fields. They report monthly mean TW3 tidal amplitudes at 110 km altitude, where a DOY 265 amplitude peak is not visible at 60N (their Figure 3).

However, the TW3 model study using the Canadian Middle Atmospheric Model by Du et al. (2010), where a monthly-mean sliding window is used to analyze internally generated 3-hourly model winds, does show an amplitude peak around DOY 265 around 100 km altitude at 60N (their figure 3). Because of this qualitative agreement with the SuperDARN observations, reference to their model study has been included in the discussion section of the revised manuscript.

Smith, A. K. (2000). Structure of the terdiurnal tide at 95 km. Geophysical Research Letters, 27(2), 177–180. doi:10.1029/1999gl010843

Akmaev, R. A. (2001). Seasonal variations of the terdiurnal tide in the mesosphere and lower thermosphere: A model study. Geophysical Research Letters, 28(19), 3817–3820. doi:10.1029/2001gl013002

Smith, A. K., & Ortland, D. A. (2001). Modeling and analysis of the structure and generation of the terdiurnal tide. Journal of the atmospheric sciences, 58(21), 3116-3134. doi:10.1175/1520-0469(2001)058<3116:MAAOTS>2.0.CO;2

Moudden, Y., & Forbes, J. M. (2013). A decade-long climatology of terdiurnal tides using TIMED/SABER observations. Journal of Geophysical Research: Space Physics, 118(7), 4534–4550. doi:10.1002/jgra.50273 Yue, J., Xu, J., Chang, L. C., Wu, Q., Liu, H.-L., Lu, X., & Russell, J. (2013). Global structure and seasonal variability of the migrating terdiurnal tide in the mesosphere and lower thermosphere. Journal of Atmospheric and Solar-Terrestrial Physics, 105-106, 191–198. doi:10.1016/j.jastp.2013.10.010

Pancheva, D., Mukhtarov, P., & Smith, A. K. (2013). Climatology of the migrating terdiurnal tide (TW3) in SABER/TIMED temperatures. Journal of Geophysical Research: Space Physics, 118(4), 1755–1767. doi:10.1002/jgra.50207

Du, J., & Ward, W. E. (2010). Terdiurnal tide in the extended Canadian Middle Atmospheric Model (CMAM). Journal of Geophysical Research: Atmospheres, 115(D24). doi:10.1029/2010jd014479

Interactive comment on Ann. Geophys. Discuss., https://doi.org/10.5194/angeo-2020-47, 2020.

Migrating tide climatologies measured by a high-latitude array of SuperDARN HF-radars

Willem E. van Caspel[1,2], Patrick J. Espy[1,2], Robert E. Hibbins[1,2], and John P. McCormack[3]

[1]Department of Physics, Norwegian University of Science and Technology (NTNU), Trondheim, Norway,
[2]Birkeland Centre for Space Science, Bergen, Norway,
[3]Space Science Division, Naval Research Laboratory, Washington DC. USA

Correspondence: W.E. van Caspel (willem.e.v.caspel@ntnu.no)

Abstract. This study uses hourly meteor wind measurements from a longitudinal array of 10 high-latitude SuperDARN HF-radars to isolate the migrating diurnal, semidiurnal and terdiurnal tid~~al mode~~s at Mesosphere-Lower-Thermosphere (MLT) altitude~~height~~s. The planetary-scale array of radars covers 180 degrees of longitude, with eight out of 10 radars being in near-continuous operation since the year 2000. Time series spanning 16 years of tidal amplitudes and phases in both zonal and meridional wind are presented, along with their respective annual climatologies. The method to isolate the migrating tid~~al mode~~s from SuperDARN meteor winds is validated using two years of winds from a high altitude meteorological analysis system~~NAVGEM-HA (Navy Global Environmental Model - High Altitude)~~. The validation steps demonstrate that, given the geographical spread of the radar stations, the derived tidal modes are most closely representative of the migrating tides at 60°N. Some of the main characteristics of the observed migrating tides are that the semidiurnal tide shows sharp phase jumps around the equinoxes and peak amplitudes during early fall~~late summer~~, and that the terdiurnal tide shows a pronounced secondary amplitude peak around DOY 265~~0~~. In addition, the diurnal tide is found to show a bi-modal circular polarization phase relation between summer and winter.

1 Introduction

Atmospheric tides are global scale waves excited primarily by radiative and latent heating effects in the troposphere and stratosphere (Chapman and Lindzen, 2012). The tides have a latitudinal spherical harmonic structure (termed Hough modes) and longitudinal zonal wavenumber (S) structure, and in the absence of dissipation their amplitudes increase exponentially with altitude due to the decreasing density of the atmosphere. In the mid- to high-latitude Mesosphere-Lower-Thermosphere (MLT), tides are an important driver of short- and long-term variability in the winds, temperatures, and densities (Smith, 2012). The migrating diurnal (DW1; for Diurnal, Westward, S=1), semidiurnal (SW2), and terdiurnal (TW3) tides are most closely tied the daily insolation cycle, following the apparent motion of the sun with a period of oscillation of 24, 12, and 8 hours, respectively. Non-migrating tides are waves whose period of oscillation are also an integer fraction of a solar day, but whose phase velocities are not sun-synchronous.

Observations capable of separating the longitudinal structure of the migrating tides from the non-migrating components have remained sparse, with the exception of satellites (e.g., Garcia et al., 2005; Ortland, 2017; Pancheva and Mukhtarov, 2011). Typical drawbacks associated with satellite measurements arise due to ~~yaw-cycle intermittency, as well as from~~ constraints imposed by asynoptic sampling (Salby, 1982), including slow local time precession and yaw cycle maneuvers. Single station tidal measurements using MF, HF, or VHF-radars have been numerous (Reid, 2015), but because they lack longitudinal coverage, the migrating and non-migrating tides are aliased to a single local wave with integer fraction of a solar day period. Such spatial aliasing is especially problematic when migrating and non-migrating tides are known to have different seasonal cycles (Sakazaki et al., 2018; Hibbins et al., 2019). A planetary-scale longitudinal chain of time-synchronized measurements can potentially bypass most, if not all, of the drawbacks associated with satellite and single station tide measurements, albeit along a single latitude. The array of SuperDARN (SD) radars used in this study is unique in that it covers 180 degrees of longitude along a latitude band centered around 60°N, and that eight of the 10 radars have been providing hourly meteor wind measurements of the MLT near-continuously since the year 2000. As a result of the simultaneous temporal and spatial sampling by the SD radars, unambiguous amplitudes and phases of the migrating diurnal, semidiurnal and terdiurnal tides can be isolated.

The following section gives a description of the data and method used to extract the migrating tides from the SD meteor winds. Section 3 presents time series spanning 16 years of hourly tidal amplitudes and phases in both the zonal and meridional winds, in addition to their respective annual climatologies. The method to extract migrating tid~~al mode~~s from the SD meteor winds is validated in section 4 by means of sampling experiments with winds obtained from the NAVGEM-HA (Navy Global Environmental Model - High Altitude) meteorological analysis system, addressing the geographical spread and changing availability in time of the SD radars. Lastly, the results are discussed in section 5.

2 Data and methodology

2.1 SuperDARN meteor winds

Figure 1 shows the geographical location and data availability between the years 2000 and 2016 of the 10 SD radars used in this study. The SD radars operate in a 10-15 MHz frequency band and are designed to measure ionospheric E- and F-region plasma phenomena. However, they also detect near-range meteor echoes in the first four range gates that can be used to determine neutral horizontal wind velocities (Hall et al., 1997). The phase shift of the return signal of each meteor echo is a measure of the component of the neutral wind velocity along the line of sight. An hourly mean horizontal wind vector is constructed from the aggregate line of sight wind vectors, over a 45 degree spread in azimuth, using a Singular Value Decomposition (SVD). While the line of sight velocities are typically very well defined (errors below 1 ms^{-1}, Chisham and Freeman, 2013), the SVD is applied only to line of sight velocities having a signal to noise ratio greater than 3.0 dB and spectral width of at most 25 ms^{-1}, to reduce contamination by sources such as auroral and sporadic E-region echoes. In addition to a hourly horizontal wind vector, the SVD also yields the standard deviation of the hourly winds, which typically ranges between 5-15 ms^{-1} for the meridional wind and 10-30 ms^{-1} for the zonal wind. The seasonal mean vertical distribution of meteor echoes as observed by the SD radars is a Gaussian centered on 102-103 km altitude, extending from approximately 75 to 125 km altitude with a full width at half maximum of 25-35 km (Chisham and Freeman, 2013; Chisham, 2018). The SD meteor winds therefore represent

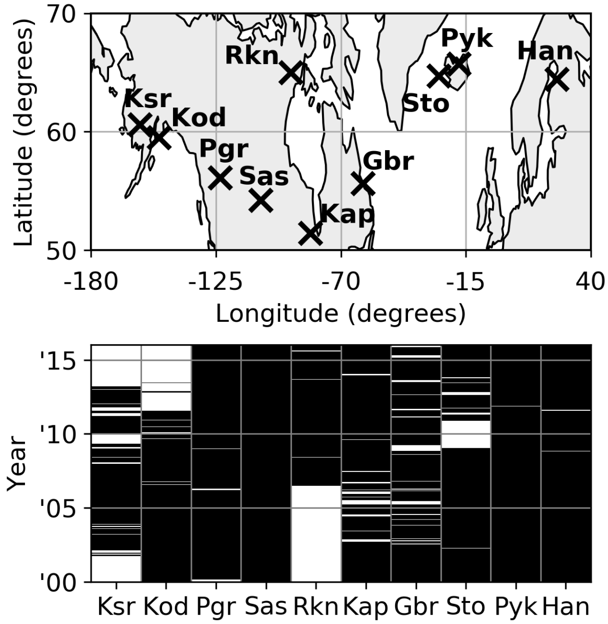

Figure 1. Abbreviated names and geographic locations (upper panel), and time of operation between the years 2000 and 2016 (black marking lower panel) of the SuperDARN radars used in this study.

a broad vertical average, which in earlier studies has been found to best correlate with neutral winds measured by traditional MF and meteor radars around 95 km altitude (Hall et al., 1997; Arnold et al., 2003).

On average each hourly SD meteor wind measurement is based on $\sim$700 meteor echoes. Before extracting the migrating tides, however, measurements based on fewer than 75 meteor echoes are discarded, as are those resulting from non-standard modes of operation. The latter amounts to discarding winds having absolute values above 100 ms^{-1} and winds fitted with a zero standard deviation (following Hibbins and Jarvis, 2008). The lower limit on the number of meteor echoes is to ensure quality of the fitted winds. Caution has been taken to ensure that no spurious tidal signals are introduced by the quality check, which may arise due to the diurnal cycle in meteor detections. This was verified by replacing all remaining data points with a value of 1 ms^{-1} and then performing spectral analysis as outlined in the following section, to confirm that tidal spectral contamination remains negligibly small.

2.2 Fourier analysis

The amplitude and phase of DW1, SW2, and TW3 are calculated by least-squares fitting the function $G(\lambda, t)$ in both space and time, where $G(\lambda, t)$ represents the migrating tidal modes along with a mean wind, given by

$$G(\lambda, t) = \sum_{k=1}^{3} A_k \sin(k\,[\Omega t - \lambda] + \phi_k) + G_0, \qquad (1)$$

where $k = 1, 2, 3$ represent DW1, SW2 and TW3, respectively, $\Omega = 2\pi/24\ \mathrm{hr}^{-1}$; λ is the geographic longitude in radians; and G_0 is the mean wind. The time development is determined by fitting $G(\lambda, t)$ over a 10-day window that is stepped forward in time with hourly steps over the range of available data. A 10-day window length is chosen such that each fit contains a proportionally sufficient number of data points to reliably extract the seasonal characteristics of the tides, without overly smoothing short-term variability.

The equidistant longitudinal spread of measurements is optimized over the range of available data to prevent skewing the fit to any particular longitude sector. ~~To that end, the radar longitude pairs of (Ksr, Kod), (Rkn, Kap), and (Sto, Pyk) are identified. If measurements are available for both stations at any given time, measurements of either one is excluded in a manner such as to optimize the equidistant longitudinal spread of measurements~~To that end, for the radar pairs closely spaced in longitude, (Ksr, Kod), (Rnk, Kap), and (Sto,Pyk), only one of each of the pairs measurements is used in the fit to Eq. 1, even if data are available for both. After performing the quality check and optimizing the longitudinal spread, fits are rejected if fewer than 960 hourly data points are present over the 10-day period, corresponding to an average continuous uptime of at least four radar stations. As a result of requiring a minimum of 960 hourly data points in each fit to Eq. 1, the estimated uncertainties on the fitted parameters become negligibly small (on the order of $0.5\ \mathrm{ms}^{-1}$ for the tidal amplitudes when employing the standard deviations of the hourly winds as an estimate of the measurement errors).

2.3 NAVGEM-HA

NAVGEM-HA is a data assimilation and modeling system that extends from the surface to the lower thermosphere. In addition to standard operational meteorological observations in the troposphere and stratosphere, NAVGEM-HA assimilates satellite-based observations of temperature, ozone and water vapor in the stratosphere, mesosphere and lower thermosphere (McCormack et al., 2017). NAVGEM-HA output is on a 1° latitude and longitude grid with a temporal frequency of 3 hours, staying above the spatial and temporal Nyquist frequency of the tides studied in this work. For comparison with ground-based instruments, vertical profiles of NAVGEM-HA analyzed winds and temperatures are converted from the model vertical grid in geopotential altitude to a geometric altitude grid. To date, NAVGEM-HA winds and tides have been shown to be in good agreement with ground-based meteor radar observations (McCormack et al., 2017; Eckermann et al., 2018; Laskar et al., 2019; Stober et al., 2019) and with independent satellite-based wind observations as reported in Dhadly et al. (2018). In the present study we employ NAVGEM-HA analyzed winds at 82.5 km altitude, staying below altitudes where effects of increased numerical diffusion imposed at the NAVGEM-HA upper boundary~~sponge layer effects~~ may impact the tides, to validate the method of extracting migrating tidal signatures from the SD meteor wind data.

3 Results

3.1 16 year time series

Figure 2 and 3 show the amplitudes and phases of the DW1, SW2, and TW3 tid~~al mode~~s retrieved from SD zonal and meridional meteor winds between the years 2000 and 2016. Here the phases are shown as the local time of maximum (LTOM), and phases for tidal amplitudes less than 1.5 ms^{-1} are not shown for sake of clarity.

SW2 shows a strongly repeatable seasonal cycle, where amplitudes peak around ~~late summer~~early fall (September - October) and mid-winter (December - January), and where sharp phase jumps occur around spring and fall equinox. The early fall~~late summer~~ amplitude maximum of SW2 typically reaches values between 19-25 ms^{-1}. In contrast, the mid-winter amplitude maximum typically lies between 10-14 ms^{-1}. SW2 consistently reaches amplitude minima coincident with the equinoctial phase jumps. While the amplitude and phase progression between the zonal and meridional components are nearly identical, meridional amplitudes can at times be 4-5 ms^{-1} larger, especially during mid-summer (June - July). In terms of its~~the~~ absolute phase separation, the meridional component of SW2 is found to lead the zonal by 2.48 hrs on average, giving it a 32 minute offset relative to a perfect circular polarization.

TW3 also shows a strongly repeatable seasonal cycle, where a broad amplitude maximum is centered on the ~~mid-~~winter half-year (October - March) and where the phase begins to shift to a later time starting October~~after DOY 250~~, stabilizes around the turn of the year~~DOY 365~~, and then shifts back to its pre-winter value up to March~~DOY 90~~. Wintertime amplitudes typically reach values between 4-6 ms^{-1}, whereas the tide is nearly non-existent throughout summer. At times the amplitude of TW3 can surpass those of SW2 and DW1, in particular around fall equinox when SW2 reaches a minimum. In addition, a pronounced secondary TW3 amplitude peak is found near Day Of Year (DOY) 265~~0~~, which can be more clearly seen in the climatology presented in the next section. This peak is most pronounced in the zonal wind, where it can reach amplitudes in the range of 4-7 ms^{-1}. In terms of its phase, TW3 is found to be nearly circularly polarized during times when the wave has an appreciable amplitude, with the meridional component leading the zonal by 1.98 hrs on average.

DW1 shows considerably more short-term and interannual variability in its amplitude, phase, and between the zonal and meridional components. This is reflected in the correlation coefficient of $r = -0.23$ between the time series of hourly zonal and meridional amplitudes of DW1, whereas for SW2 and TW3 this is $r = 0.90$ and $r = 0.66$, respectively. There is, however, a clear seasonal cycle present in both the amplitude and phase of DW1, which can be more clearly seen in the climatology presented in the next section.

3.2 Climatologies

Figure 4 shows the yearly amplitude and phase climatologies of DW1, SW2, and TW3 based on the amplitudes and phases presented in the previous section. The climatologies are constructed by calculating the mean amplitude and phase for each DOY, where the mean phase is calculated using the circular mean (Fisher, 1995). The shaded area represents the standard deviation around the climatological mean amplitude and serves as a measure of year-to-year variability.

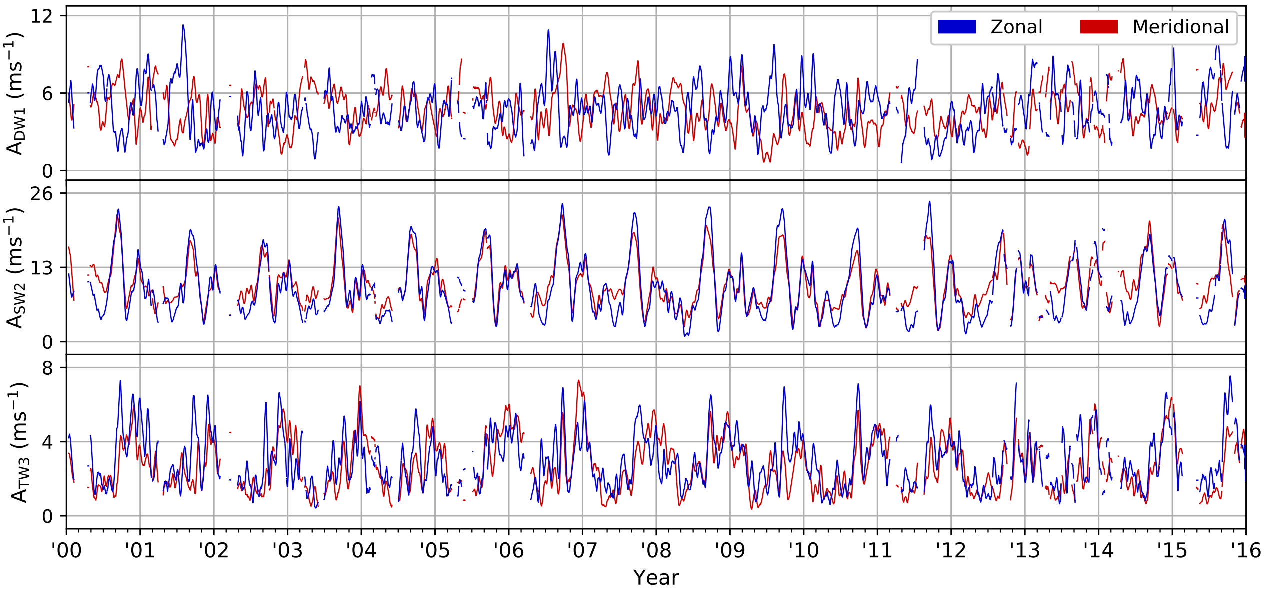

Figure 2. Amplitude of DW1 (top), SW2 (middle), and TW3 (bottom) in SuperDARN zonal (red) and meridional (blue) meteor winds between the years 2000 and 2016.

For the zonal (meridional) component, the climatological amplitude of SW2 in early fall~~late summer~~ and mid-winter peaks at 20.7 (18.8) ms^{-1} and 12.4 (12.4) ms^{-1}, respectively. Variability around the climatological mean of SW2 is largely constant throughout the year, with an average standard deviation of 2.2 (2.0) ms^{-1}. For TW3, ~~mid-~~wintertime zonal (meridional) amplitudes peak at 4.4 (5.1) ms^{-1}, while the DOY 265~~0~~ amplitude peaks at 5.3 (4.1) ms^{-1}. The average standard deviation of the amplitude of TW3 is 1.0 (0.9) ms^{-1}, while variability around the climatological mean is highest coincident with the amplitude peak at DOY 265~~0~~ by 1.7 (1.4) ms^{-1}.

The climatology of DW1 stands out in that amplitudes in the meridional wind broadly tend to maximize around 6.7 ms^{-1} near the equinoxes, whereas those in the zonal wind maximise around 6.7 ms^{-1} near the solstices. In addition, the climatological phase shows a circular polarization where the zonal component leads the meridional by approximately 6 hrs during the~~fall and~~ winter half-year, but lags it by approximately 6 hrs during the~~spring and~~ summerhalf-year. The climatological phase thus shows a bi-modal circular polarization, with the polarization flipping sign broadly between summer and winter~~during the summer months~~. Variability around the climatological amplitude of the zonal (meridional) component of DW1 stays largely constant throughout the year, with an average standard deviation of 1.6 (1.3) ms^{-1}.

4 Validation

In this section sampling experiments with NAVGEM-HA are used to validate the method to extract migrating tides from the longitudinal chain of SD meteor wind measurements. The sampling experiments seek to address the geographical spread of

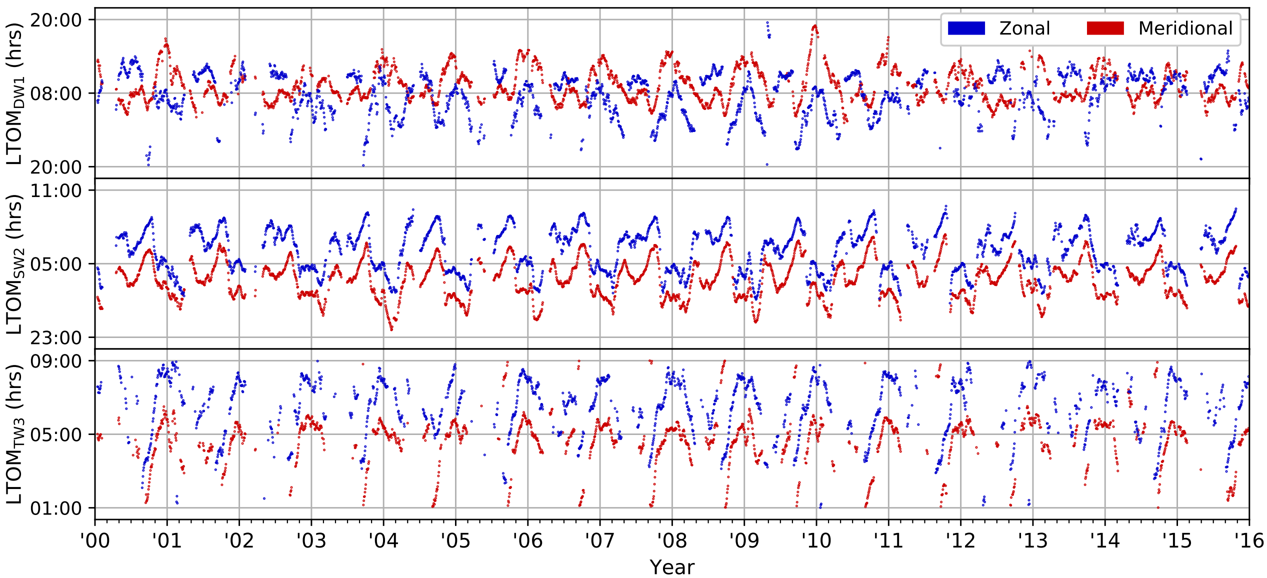

Figure 3. Phase of DW1 (top), SW2 (middle), and TW3 (bottom) in SuperDARN zonal (red) and meridional (blue) meteor winds between the years 2000 and 2016. Phases are plotted as the local time of maximum (LTOM). Only phases for when tidal amplitudes are greater than 1.5 ms^{-1} are shown for ~~sake of~~ clarity.

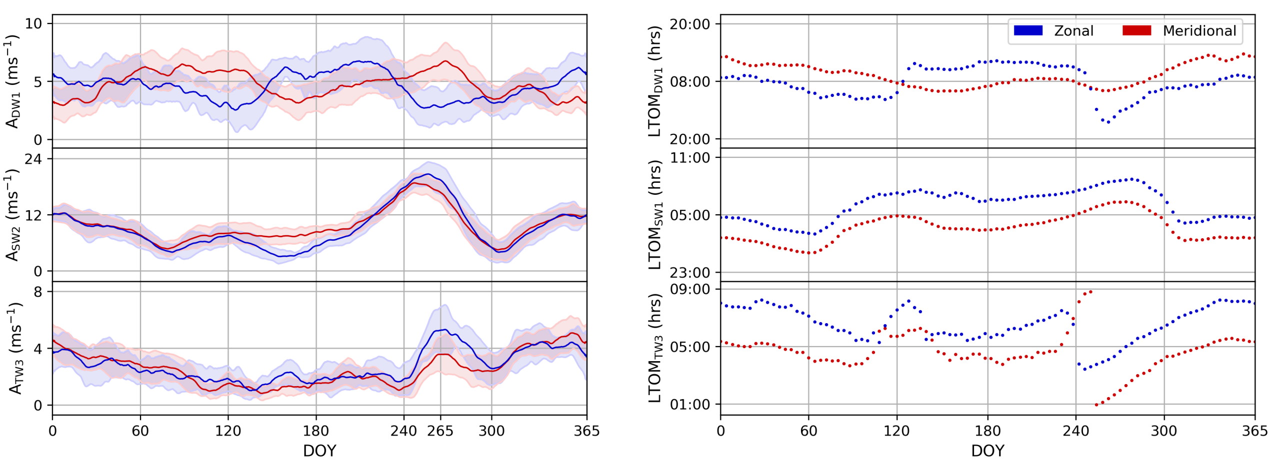

Figure 4. Climatologies of the amplitude (left panels) and phase (right panels) of the DW1 (top), SW2 (middle), and TW3 (bottom) based on SuperDARN meridional (red) and zonal (blue) meteor winds between the years 2000 and 2016. Shading marks the standard deviation around the climatological mean. The amplitude of TW3 on DOY 265, referenced extensively in the text, is indicated in the bottom left panel.

the SD stations, as well as the spatial sampling variations due to the changing availability of the individual stations with time (as shown in Figure 1). Cross-contamination errors arising from the geographical spread of the SD stations are expected to be large relative to the error propagating from any individual measurement uncertainties, since each tidal fit includes at least 960 hourly data points, as discussed in section 2.2.

4.1 Geographical spread

To address the geographical spread of the SD stations, migrating tides (Eq. 1) are fitted to NAVGEM-HA meridional winds sampled at the locations of available SD measurements (NAVGEM-SD), after quality checking and optimizing the longitudinal spread as discussed in section 2.2. These are then compared against those fitted to a full longitude circle of data taken along 60°N (NAVGEM-360). Fits along a full longitude circle are orthogonal to any other longitudinal waves, and so form a benchmark of the 'true' migrating tides. As with the fits to SD, a 10-day time window is used where the window is now stepped forward in 3 hourly steps to accommodate the temporal resolution of NAVGEM-HA.

Figure 5 shows the migrating tidal modes derived from NAVGEM-SD and NAVGEM-360 for the years 2014 and 2015, demonstrating that there is no structural deviation between the two for all three tidal components. The largest amplitude deviations remain incidental, whereas the phases are in close agreement at all times. On average, the phase difference between NAVGEM-SD and NAVGEM-360 is 5.9, 5.6 and 6.0 minutes for DW1, SW2, and TW3, respectively. The geographical spread of the SD radars is therefore concluded to not lead to significant cross-contamination errors between the tidal modes representative of the (global) migrating tides.

The corresponding tides measured by the array of SD radars are also shown in Figure 5 (green curves). These are, however, not intended to serve as a detailed comparison between the modeled and observed tides. For such a comparison the top level of the NAVGEM-HA system would have to be extended past the vertical extent of the SD meteor echo distribution ($\sim$ 125 km), which is beyond the scope of the current work. Nevertheless, the SW2 and TW3 tides from SD and NAVGEM-HA at 82.5 km share similar characteristics in their seasonal amplitude and phase cycle, supporting the use of NAVGEM-HA to validate the SD tidal analysis method. A possible reason for the difference between the modeled and observed DW1 tide is discussed in section 5.

4.2 Root mean square error analysis

To examine the quality of the tides fitted to NAVGEM-SD, they are compared to those fitted to NAVGEM-360 by looking at the root-mean-square error (RMSE) between their respective tidal fields. Here the tidal fields themselves can be fully reconstructed on a 360 degree longitude-time grid using the 3 hourly fitted amplitudes and phases. To account for the changing availability of the SD stations with time, the RMSE is reported using 2014 NAVGEM-HA meridional winds sampled at the locations of active SD stations for each year between 2000 and 2016. The resulting year-by-year RMSE values, calculated between the yearly reconstructed tidal fields of NAVGEM-SD and NAVGEM-360, are shown in Figure 6. For each year the RMSE is comparatively low relative to the absolute tidal amplitudes shown in Figure 5, assuring the validity of the method to extract the migrating tides over the range of hourly SD data used in this study. It also shows that the stations changing with time does not induce any substantial long-term trends.

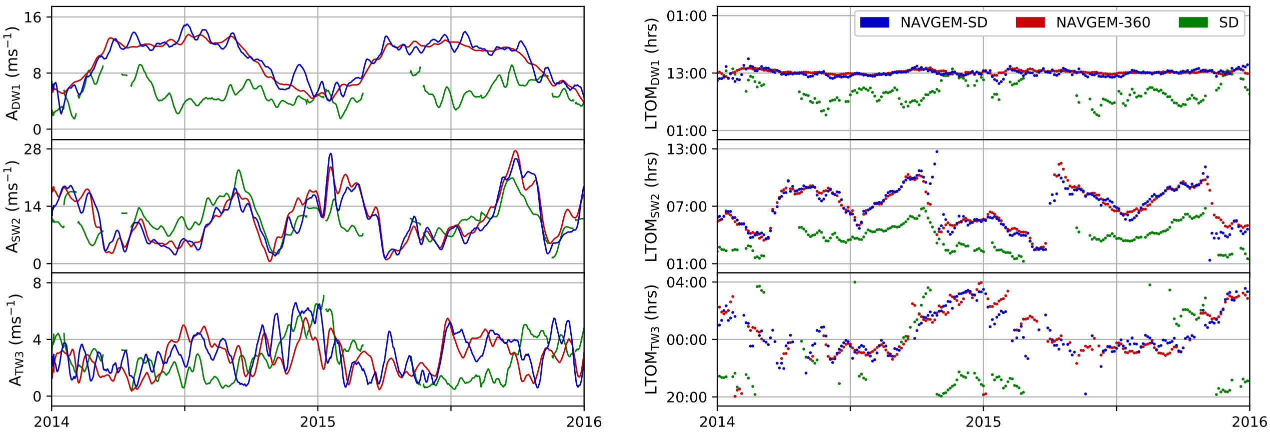

Figure 5. Amplitude and phase of DW1 (top), SW2 (middle) and TW3 (bottom) in NAVGEM-SD (blue) and NAVGEM-360 (red) meridional winds at 82.5 km altitude for the years 2014 and 2015. Phases are plotted as local time of maximum (LTOM). Green curves show the corresponding meridional tides from around 95 km altitude as measured by the array of SuperDARN (SD) radars.

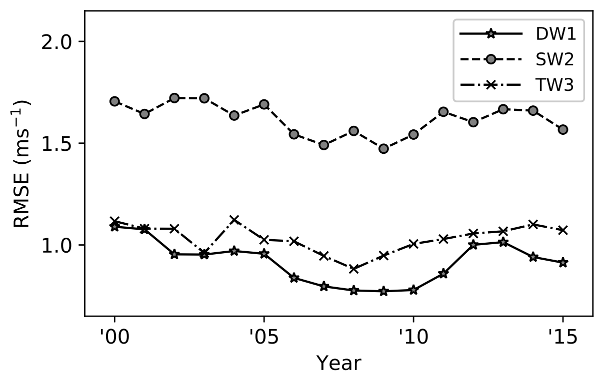

Figure 6. Yearly RMSE between the tidal fields constructed from fits to NAVGEM-360 and NAVGEM-SD sampled at active SuperDARN stations for each year between 2000 and 2016.

In the above, sampling NAVGEM-360 at 60°N i~~was~~ motivated by NAVGEM-SD most closely corresponding to NAVGEM-360 at this latitude, which is now demonstrated. To that end, the RMSE is examined between NAVGEM-SD and NAVGEM-360, where the latter is taken at each latitude between 52°N and 68°N. Figure 7 demonstrates that the RMSE for the SW2 and TW3 tidal fields reaches a clear minimum at 60°N, while the RMSE of DW1 decreases also for latitudes greater than 60°N. However, the relative difference between the RMSE of DW1 at 60°N and 68°N is comparatively low (-2.4%). The migrating tides extracted from NAVGEM-SD are therefore concluded to most closely correspond to those at 60°N. Following this conclusion, the migrating tides extracted from SD are taken to be most closely representative of those at 60°N.

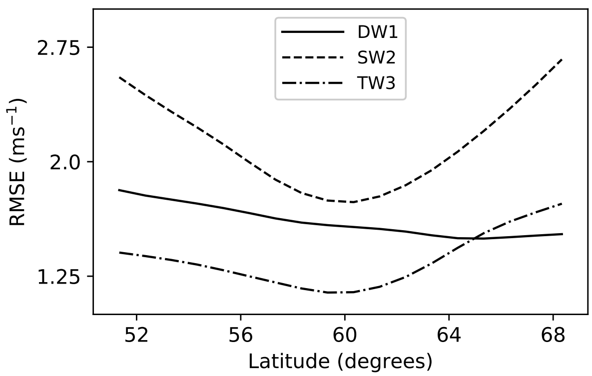

Figure 7. Yearly RMSE between the tidal fields constructed from fits to 2014 NAVGEM-SD and NAVGEM-360 taken along each latitude between 52°N and 68°N.

5 Discussion

The SW2 and TW3 tidal modes isolated from 16 years of SD meteor winds show a well-defined and strongly recurring seasonal cycle. The main features of SW2, namely its amplitude peaks around redearly falllate summer and mid-winter, and sharp phase jumps around the equinoxes, are in qualitative agreement with previous observational and model studies of the mid- and high-latitude migrating semidiurnal tide (Wu et al., 2011; Xu et al., 2011; Forbes and Vial, 1989). The SW2 presented in this work indicates that the early falllate summer amplitude peaks in the zonal and meridional winds are significantly higher than those in mid-winter, by 71% and 56% on average, respectively.

The seasonal cycle of TW3, showing a broad wintertime amplitude maximum and a near 4-hour LTOM phase progression tracing a half-circle throughout winter, is also in qualitative agreement with previous (satellite) observational and model studies of the mid- and high-latitude migrating terdiurnal tide (Smith, 2000; Akmaev, 2001; Smith and Ortland, 2001). The pronounced amplitude peak around DOY 2650 observed byin SD uniquely stands out, however, possibly owing to the high temporal resolution offered by the radars. The DOY 2650 amplitude peak appears to be an enhancement superimposed on the broad wintertime maximum. There are a number of mechanisms that can excite a time-localized forcing of TW3, such as non-linear wave-wave interactions and diurnal tide and gravity wave interactions (Teitelbaum et al., 1989; Miyahara and Forbes, 1991). WhetherIf conditions are favourable for any such mechanisms to come into effect around DOY 2650 remains to be examined. Here we note that a similar time-localized amplitude peak has been described in the zonal and meridional winds above 100 km altitude at 60°N in the Canadian Middle Atmosphere Model (CMAM) (Du and Ward, 2010). Further, Here we note that traditional single point radar measurements of the 8 hour wave are prone to contamination by gravity waves, for which eight hours falls in the middle of the typical mid- to high-latitude spectrum at MLT heights (e.g., Conte et al., 2018). Gravity wave contamination is expected to be comparatively low for the TW3 tidal mode retrieved from SD, however, since the horizontal scale of gravity waves is much smaller than the longitudinal extent covered by the radars.

The DW1 tidal mode shows considerably more short-term and interannual variability, and a different seasonal behavior between the zonal and meridional component. A possible cause of this is that DW1 has a relatively short vertical wavelength. Whereas the semidiurnal and terdiurnal tides have a vertical wavelength on the order of 100 km in the MLT (Chapman and Lindzen, 2012; Yuan et al., 2008; Smith, 2000), the diurnal tide has a vertical wavelength on the order of 25-35 km (e.g., Avery et al., 1989). The vertical wavelength of DW1 is therefore much nearer to the vertical average represented by the SD meteor winds, which can cause DW1 to partly cancel out over the meteor echo range. In addition, DW1 is the tidal mode most susceptible to contamination by non-migrating tides, given that the 180 degrees of longitude aliases DW1 and the diurnal oscillation in the mean wind (D0). Although no evidence of such cross-contamination is found in the NAVGEM-HA sampling experiments, and D0 amplitudes in NAVGEM-HA (NAVGEM-360) never reach above 4.0 ms^{-1} at this latitude. Lastly, DW1 is likely to be the tidal mode that is most strongly affected by the diurnal cycle of meteor echoes. Neveronetheless, the climatology of the meridional component of DW1 shows close agreement with the seasonal cycle of the anti-symmetric diurnal (1,1) Hough-mode calculated from TIMED Doppler Interferometer (TIDI) and NAVGEM-HA meridional winds by Dhadly et al. (2018). It is possible that certain diurnal modes are selectively filtered by SD based on their respective vertical wavelength and that the (1,1) mode is the dominant remaining mode, even though the amplitude of this mode broadly peaks around 25°N (Chapman and Lindzen, 2012). Future work could go out to investigating if the climatology of the zonal component of DW1 in SD can also be associated with the diurnal (1,1) Hough mode.

6 Conclusion

This study has leveraged the longitudinal coverage of 10 high-latitude SuperDARN (SD) radars to isolate the DW1, SW2, and TW3 tidal modes from 16 years of hourly meteor wind measurements of the mid- to high-latitude MLT. Based on sampling experiments with NAVGEM-HA, it is demonstrated that the SD tidal modes are closely representative of the (global) migrating tides along 60°N. The amplitude and phase structure of SW2 and TW3 show a strongly recurring seasonal cycle, whereas DW1 shows considerably more year-to-year variability. Notable observations are that the climatological early falllate summer amplitude maximum of SW2 in the zonal (meridional) wind is 8.3 (6.4) ms^{-1} greater than the mid-winter maximum, and that TW3 is marked by a secondary amplitude peak around DOY 2650 that reaches values of 5.3 $\pm$ 1.7 ms^{-1} in the zonal wind. In addition, DW1 is found to show a bi-modal circular phase polarization relation, where the zonal component leads the meridional during most of the year and vice versa during summer.

Many open questions remain in terms of how tidal variability is coupled to variability in their forcing mechanisms and propagation conditions. For future work, the time series of validated SD tidal measurements presented in this work can serve as a valuable source of data in studying the long- and short-term trends and variability of the migrating tides in the high-latitude MLT. The method and validation steps outlined in this work will also contribute to similar analyses of SD meteor winds from the continuously expanding global network of radars.

Author contributions. WEC, PJE and REH developed the concept, while WEC performed the data analysis and wrote the paper. JPM provided the NAVGEM-HA data and contributed section 2.3. PJE, REH and JPM gave feedback on the conceptual development and draft versions of this work.

Competing interests. The authors declare that no competing interests are present.

Acknowledgements. The authors acknowledge the use of the SuperDARN meteor wind data product. The SuperDARN project is funded by national scientific funding agencies of Australia, China, Canada, France, Japan, Italy, Norway, South Africa, the United Kingdom, and the United States. Data are available from Virginia Tech at vt.superdarn.org. Development of NAVGEM-HA was supported by the Chief of Naval Research and the Department of Defense High Performance Computing Modernization Project. The authors thank two anonymous reviewers for their assistance in improving this work.

The current research was partly funded by the Research Council of Norway/CoE under contract 223525/F50.

References

Akmaev, R. A.: Seasonal variations of the terdiurnal tide in the mesosphere and lower thermosphere: A model study, Geophysical Research Letters, 28, 3817–3820, https://doi.org/10.1029/2001gl013002, 2001.

Arnold, N. F., Cook, P. A., Robinson, T. R., Lester, M., Chapman, P. J., and Mitchell, N.: Comparison of D-region Doppler drift winds measured by the SuperDARN Finland HF radar over an annual cycle using the Kiruna VHF meteor radar, Annales Geophysicae, 21, 2073–2082, https://doi.org/10.5194/angeo-21-2073-2003, 2003.

Avery, S., Vincent, R., Phillips, A., Manson, A., and Fraser, G.: High-latitude tidal behavior in the mesosphere and lower thermosphere, Journal of Atmospheric and Terrestrial Physics, 51, 595–608, https://doi.org/10.1016/0021-9169(89)90057-3, 1989.

Chapman, S. and Lindzen, R. S.: Atmospheric tides: thermal and gravitational, Springer Science & Business Media, 2012.

Chisham, G.: Calibrating SuperDARN Interferometers Using Meteor Backscatter, Radio Science, 53, 761–774, https://doi.org/10.1029/2017rs006492, 2018.

Chisham, G. and Freeman, M. P.: A reassessment of SuperDARN meteor echoes from the upper mesosphere and lower thermosphere, Journal of Atmospheric and Solar-Terrestrial Physics, 102, 207–221, https://doi.org/10.1016/j.jastp.2013.05.018, 2013.

Conte, J. F., Chau, J. L., Laskar, F. I., Stober, G., Schmidt, H., and Brown, P.: Semidiurnal solar tide differences between fall and spring transition times in the Northern Hemisphere, Annales Geophysicae, 36, 999–1008, https://doi.org/10.5194/angeo-36-999-2018, 2018.

Dhadly, M. S., Emmert, J. T., Drob, D. P., McCormack, J. P., and Niciejewski, R. J.: Short-Term and Interannual Variations of Migrating Diurnal and Semidiurnal Tides in the Mesosphere and Lower Thermosphere, Journal of Geophysical Research: Space Physics, 123, 7106–7123, https://doi.org/10.1029/2018ja025748, 2018.

Du, J. and Ward, W. E.: Terdiurnal tide in the extended Canadian Middle Atmospheric Model (CMAM), Journal of Geophysical Research: Atmospheres, 115, https://doi.org/10.1029/2010jd014479, 2010.

Eckermann, S. D., Ma, J., Hoppel, K. W., Kuhl, D. D., Allen, D. R., Doyle, J. A., Viner, K. C., Ruston, B. C., Baker, N. L., Swadley, S. D., Whitcomb, T. R., Reynolds, C. A., Xu, L., Kaifler, N., Kaifler, B., Reid, I. M., Murphy, D. J., and Love, P. T.: High-Altitude (0–100 km) Global Atmospheric Reanalysis System: Description and Application to the 2014 Austral Winter of the Deep Propagating Gravity Wave Experiment (DEEPWAVE), Monthly Weather Review, 146, 2639–2666, https://doi.org/10.1175/mwr-d-17-0386.1, 2018.

Fisher, N. I.: Statistical analysis of circular data, cambridge university press, 1995.

Forbes, J. and Vial, F.: Monthly simulations of the solar semidiurnal tide in the mesosphere and lower thermosphere, Journal of Atmospheric and Terrestrial Physics, 51, 649–661, https://doi.org/10.1016/0021-9169(89)90063-9, 1989.

Garcia, R. R., Lieberman, R., Russell, J. M., and Mlynczak, M. G.: Large-Scale Waves in the Mesosphere and Lower Thermosphere Observed by SABER, Journal of the Atmospheric Sciences, 62, 4384–4399, https://doi.org/10.1175/jas3612.1, 2005.

Hall, G. E., MacDougall, J. W., Moorcroft, D. R., St.-Maurice, J.-P., Manson, A. H., and Meek, C. E.: Super Dual Auroral Radar Network observations of meteor echoes, Journal of Geophysical Research: Space Physics, 102, 14 603–14 614, https://doi.org/10.1029/97ja00517, 1997.

Hibbins, R. E. and Jarvis, M. J.: A long-term comparison of wind and tide measurements in the upper mesosphere recorded with an imaging Doppler interferometer and SuperDARN radar at Halley, Antarctica, Atmospheric Chemistry and Physics, 8, 1367–1376, https://doi.org/10.5194/acp-8-1367-2008, 2008.

Hibbins, R. E., Espy, P. J., Orsolini, Y. J., Limpasuvan, V., and Barnes, R. J.: SuperDARN Observations of Semidiurnal Tidal Variability in the MLT and the Response to Sudden Stratospheric Warming Events, Journal of Geophysical Research: Atmospheres, 124, 4862–4872, https://doi.org/10.1029/2018jd030157, 2019.

Laskar, F. I., McCormack, J. P., Chau, J. L., Pallamraju, D., Hoffmann, P., and Singh, R. P.: Interhemispheric Meridional Circulation During Sudden Stratospheric Warming, Journal of Geophysical Research: Space Physics, 124, 7112–7122, https://doi.org/10.1029/2018ja026424, 2019.

McCormack, J., Hoppel, K., Kuhl, D., de Wit, R., Stober, G., Espy, P., Baker, N., Brown, P., Fritts, D., Jacobi, C., Janches, D., Mitchell, N., Ruston, B., Swadley, S., Viner, K., Whitcomb, T., and Hibbins, R.: Comparison of mesospheric winds from a high-altitude meteorological analysis system and meteor radar observations during the boreal winters of 2009–2010 and 2012–2013, Journal of Atmospheric and Solar-Terrestrial Physics, 154, 132–166, https://doi.org/10.1016/j.jastp.2016.12.007, 2017.

Miyahara, S. and Forbes, J. M.: Interactions between Gravity Waves and the Diurnal Tide in the Mesosphere and Lower Thermosphere, Journal of the Meteorological Society of Japan. Ser. II, 69, 523–531, https://doi.org/10.2151/jmsj1965.69.5_523, 1991.

Ortland, D. A.: Daily estimates of the migrating tide and zonal mean temperature in the mesosphere and lower thermosphere derived from SABER data, Journal of Geophysical Research: Atmospheres, 122, 3754–3785, https://doi.org/10.1002/2016jd025573, 2017.

Pancheva, D. and Mukhtarov, P.: Atmospheric Tides and Planetary Waves: Recent Progress Based on SABER/TIMED Temperature Measurements (2002–2007), in: Aeronomy of the Earth's Atmosphere and Ionosphere, pp. 19–56, Springer Netherlands, https://doi.org/10.1007/978-94-007-0326-1_2, 2011.

Reid, I. M.: MF and HF radar techniques for investigating the dynamics and structure of the 50 to 110 km height region: a review, Progress in Earth and Planetary Science, 2, https://doi.org/10.1186/s40645-015-0060-7, 2015.

Sakazaki, T., Fujiwara, M., and Shiotani, M.: Representation of solar tides in the stratosphere and lower mesosphere in state-of-the-art reanalyses and in satellite observations, Atmospheric Chemistry and Physics, 18, 1437–1456, https://doi.org/10.5194/acp-18-1437-2018, 2018.

Salby, M. L.: Sampling Theory for Asynoptic Satellite Observations. Part I: Space-Time Spectra, Resolution, and Aliasing, Journal of the Atmospheric Sciences, 39, 2577–2600, https://doi.org/10.1175/1520-0469(1982)039<2577:STFASO>2.0.CO;2, 1982.

Smith, A. K.: Structure of the terdiurnal tide at 95 km, Geophysical Research Letters, 27, 177–180, https://doi.org/10.1029/1999gl010843, 2000.

Smith, A. K.: Global Dynamics of the MLT, Surveys in Geophysics, 33, 1177–1230, https://doi.org/10.1007/s10712-012-9196-9, 2012.

Smith, A. K. and Ortland, D. A.: Modeling and Analysis of the Structure and Generation of the Terdiurnal Tide, Journal of the Atmospheric Sciences, 58, 3116–3134, https://doi.org/10.1175/1520-0469(2001)058<3116:MAAOTS>2.0.CO;2, 2001.

Stober, G., Baumgarten, K., McCormack, J. P., Brown, P., and Czarnecki, J.: Comparative study between ground-based observations and NAVGEM-HA reanalysis data in the MLT region, https://doi.org/10.5194/acp-2019-1006, 2019.

Teitelbaum, H., Vial, F., Manson, A., Giraldez, R., and Massebeuf, M.: Non-linear interaction between the diurnal and semidiurnal tides: terdiurnal and diurnal secondary waves, Journal of Atmospheric and Terrestrial Physics, 51, 627–634, https://doi.org/10.1016/0021-9169(89)90061-5, 1989.

Wu, Q., Ortland, D., Solomon, S., Skinner, W., and Niciejewski, R.: Global distribution, seasonal, and inter-annual variations of mesospheric semidiurnal tide observed by TIMED TIDI, Journal of Atmospheric and Solar-Terrestrial Physics, 73, 2482–2502, https://doi.org/10.1016/j.jastp.2011.08.007, 2011.

Xu, X., Manson, A. H., Meek, C. E., Jacobi, C., Hall, C. M., and Drummond, J. R.: Mesospheric wind semidiurnal tides within the Canadian Middle Atmosphere Model Data Assimilation System, Journal of Geophysical Research, 116, https://doi.org/10.1029/2011jd015966, 2011.

Yuan, T., Schmidt, H., She, C. Y., Krueger, D. A., and Reising, S.: Seasonal variations of semidiurnal tidal perturbations in mesopause region temperature and zonal and meridional winds above Fort Collins, Colorado (40.6°N, 105.1°W), Journal of Geophysical Research, 113, https://doi.org/10.1029/2007jd009687, 2008.